PNAS RESEARCH ARTICLE | PHYSICS

Generic character of charge and spin density waves in superconducting cuprates

Sangjun Lee[a,b,1], Edwin W. Huang[a,c,1], Thomas A. Johnson[a,b,1], Xuefei Guo[a,b], Ali A. Husain[a,b], Matteo Mitrano[a,b], Kannan Lu[a,b], Alexander V. Zakrzewski[a,b], Gilberto A. de la Peña[a,b], Yingying Peng[a,b], Hai Huang[d], Sang-Jun Lee[d], Hoyoung Jang[d], Jun-Sik Lee[d], Young Il Joe[e], William B. Doriese[e], Paul Szypryt[e], Daniel S. Swetz[e], Songxue Chi[f], Adam A. Aczel[f], Gregory J. MacDougall[a,b,2], Steven A. Kivelson[g], Eduardo Fradkin[a,c,2], and Peter Abbamonte[a,b,2]

Edited by J. C. Davis, University of Oxford, Oxford, United Kingdom; received October 23, 2021; accepted February 10, 2022

Charge density waves (CDWs) have been observed in nearly all families of copper-oxide superconductors. But the behavior of these phases across different families has been perplexing. In La-based cuprates, the CDW wavevector is an increasing function of doping, exhibiting the so-called Yamada behavior, while in Y- and Bi-based materials the behavior is the opposite. Here, we report a combined resonant soft X-ray scattering (RSXS) and neutron scattering study of charge and spin density waves in isotopically enriched $La_{1.8-x}Eu_{0.2}Sr_xCuO_4$ over a range of doping $0.07 \leq x \leq 0.20$. We find that the CDW amplitude is temperature independent and develops well above experimentally accessible temperatures. Further, the CDW wavevector shows a nonmonotonic temperature dependence, exhibiting Yamada behavior at low temperature with a sudden change occurring near the spin ordering temperature. We describe these observations using a Landau–Ginzburg theory for an incommensurate CDW in a metallic system with a finite charge compressibility and spin-CDW coupling. Extrapolating to high temperature, where the CDW amplitude is small and spin order is absent, our analysis predicts a decreasing wavevector with doping, similar to Y and Bi cuprates. Our study suggests that CDW order in all families of cuprates forms by a common mechanism.

charge density waves | spin density waves | cuprates | high-temperature superconductivity

Charge density waves (CDWs) are pervasive in cuprate superconductors and are now believed to be fundamental to the low-temperature properties of these materials. A perplexing issue has been that the evolution of the wavevector of the CDW, Q_{CDW}, upon doping has different trends in different material families (1). In $YBa_2Cu_3O_{6+\delta}$ (YBCO) (2–4) and Bi-based cuprates (5–7) Q_{CDW} decreases with increasing doping, while La-based cuprates (8–10) exhibit the so-called Yamada relationship (11) in which Q_{CDW} increases with doping, x, as $Q_{\mathrm{CDW}} = 2x$ for $x \leq 0.125$ and saturates at $Q_{\mathrm{CDW}} = 0.25$ for $x > 0.125$. This disparity raises the question of whether the CDWs in different cuprates are fundamentally different or whether there is an underlying generic origin of CDW order that simply manifests in different ways for material-specific reasons.

The observed Q_{CDW} at a given doping and temperature, T, may be influenced by many factors, such as pinning on the lattice or other types of order that may also be present (12–14). Such extrinsic effects may cause Q_{CDW} to shift away from its intrinsically favored "natural" value. Thus, it is essential to identify and disentangle the various effects that interact with the CDW. In particular, a spin density wave (SDW) is present in La cuprates that is absent in YBCO and Bi cuprates, suggesting that the presence of spin order may be a key factor in the distinct behaviors of Q_{CDW} in these materials (12–14). A close relationship between SDW and CDW order was previously observed in stripe-ordered nickelates (15) where Q_{CDW} is influenced by commensuration with the lattice and pinning with the SDW. What enabled these effects to be disentangled was a full study of the doping and temperature dependence, $Q_{\mathrm{CDW}}(x, T)$ (15), and a similar strategy could shed light on the cuprates. The La cuprates are in some ways ideal for this; they have strong CDW and SDW instabilities, and the concentration of doped holes may be readily measured and varied across the entire range of the superconducting dome. However, La cuprates have the complication of a low-temperature tetragonal (LTT) distortion whose onset temperature is similar to that of the CDW.

Here, using resonant soft X-ray scattering (RSXS) and neutron scattering, we present a study of the CDW and SDW in $La_{1.8-x}Eu_{0.2}Sr_xCuO_4$ (LESCO) over a wide range of doping $0.07 \leq x \leq 0.20$ and temperatures up to 270 K. We used isotopically enriched LESCO crystals with ^{153}Eu for the neutron measurements to reduce the neutron absorption cross-section, giving us improved sensitivity to the SDW (Materials and Methods). LESCO has the advantage over other La cuprates that the LTT transition temperature is

Significance

The essential physics of the cuprate high-temperature superconductors have been a central focus of condensed-matter physics for more than three decades. Although initially controversial, it is now clear that a ubiquitous tendency toward charge-density-wave (CDW) order is intertwined with the superconductivity. However, this manifests differently in distinct cuprates. On the basis of extensive X-ray and neutron scattering studies of the temperature and doping dependence of the CDW and spin-density-wave (SDW) correlations in one representative cuprate and a comparison with existing studies on other cuprates, we show that there plausibly is a single, preferred CDW order at the microscale, whose manifestation at low temperatures is modified in predictable ways by material-specific details, including its interaction with SDW order.

The authors declare no competing interest.

This article is a PNAS Direct Submission.

[1]S.L., E.W.H., and T.A.J. contributed equally to this work.

[2]To whom correspondence may be addressed. Email: abbamont@illinois.edu, efradkin@illinois.edu, or gmacdoug@illinois.edu.

This article contains supporting information online at https://www.pnas.org/lookup/suppl/doi:10.1073/pnas.2119429119/-/DCSupplemental.

Published April 4, 2022.

almost fixed to $T_{\mathrm{LTT}} \sim 130$ K over the whole phase diagram (16, 17). Hence, while the LTT distortion may influence the CDW, it at least does not change with doping, simplifying the interpretation. RSXS measurements were performed on LESCO crystals with $x = 0.07$, 0.10, 0.125, 0.15, 0.17, 0.20 and the CDW was observed in all dopings except for $x = 0.07$. Neutron scattering measurements were performed on $x = 0.07, 0.10, 0.11$, 0.125, 0.15 and the SDW was observed in all dopings.

We find, at low temperature, that the SDW and CDW in LESCO exhibit the expected Yamada behavior (11), consistent with previous findings for the CDW (18). At higher temperatures, however, the CDW exhibits two distinct behaviors. First, the CDW does not show a clear phase transition. As previously demonstrated in ref. 19 for $x = 0.125$, while the CDW peak intensity decreases with temperature, its integrated intensity is constant over the entire temperature range measured. We find that this behavior obtains for all dopings, implying that the CDW amplitude is approximately temperature independent everywhere in the phase diagram where the CDW is present. Using a nonlinear sigma model, we show that this behavior is consistent with a CDW with very high mean-field transition temperature (far above room temperature) in the presence of weak, quenched disorder that induces phase fluctuations without significantly altering the CDW amplitude.

Second, we find that Q_{CDW} exhibits a complicated, nonmonotonic dependence on doping and temperature, consistent with a competition between multiple effects. We explain this behavior quantitatively using a Landau–Ginzburg theory with a different ingredient, the compressibility of the uncondensed metallic electrons (20), which competes with the natural Q_{CDW} as well as its pinning on the SDW. Using this theory, the experimental results can be extrapolated to high temperatures, where extrinsic effects are minimal, identifying an "intrinsic" Q_{CDW} that decreases with increasing x and is quantitatively similar to the ordering vectors in YBCO and Bi cuprates. This finding suggests that the CDW in La-based cuprates is characterized by higher temperature/energy scales than previously appreciated and that CDW order has a common origin in all cuprates but manifests differently at low temperature due to material-specific details.

Starting with the neutron data, clear SDW peaks that disappear with increasing temperature were observed in all samples studied. Fig. 1*A* shows elastic momentum scans for the case of LESCO with $x = 0.125$ (see *SI Appendix*, section III for a wider scan). The integrated intensity of this peak, determined from a Gaussian fit, is plotted against temperature in Fig. 1*B*, and the shift of the SDW incommensuration, δ, is illustrated in Fig. 1*C*. To define the onset temperature, T_{SDW}, for each doping, we fit the intensity to the function $I(T) = I_0[1 - (T/T_{\mathrm{SDW}})^2] + C$ (for $T \leq T_{\mathrm{SDW}}$). This function is likely to underestimate T_{SDW} if the transition is broadened (*SI Appendix*, section III), but is useful for comparing different samples. (See Figs. 4 and 6, respectively, for the resulting values of T_{SDW} and δ.) We make two key observations. First, the inferred SDW wavevector is temperature independent, with a doping dependence following the well-known Yamada relation (11), where $\delta \sim x$ until saturation above $x = 0.125$. Second, we find $T_{\mathrm{SDW}} = 11$ K for $x = 0.07$, while $T_{\mathrm{SDW}} \sim 40$ K for the other dopings (*SI Appendix*, section III), which is consistent with the neutron scattering result for $x = 0.15$ from ref. 21.

Turning now to the CDW, RSXS scans of the CDW peak profiles for $0.10 \leq x \leq 0.20$ at selected temperatures are shown in Fig. 2*A*. We find that the CDW onset is very broad in temperature, without a clear phase transition, and is visible even at the highest temperature measured ($T = 270$ K for $x = 0.15$). Further, the CDW peak center (black ticks in Fig. 2*A*) exhibits

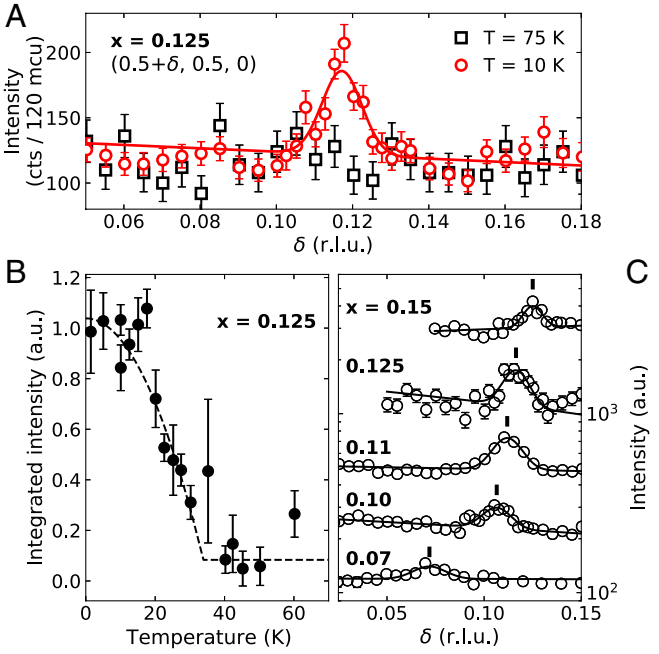

Fig. 1. Neutron scattering measurements of the spin order in isotopically enriched LESCO crystals. (*A*) Momentum scan in the *H* direction for $x = 0.125$, at temperatures above and below T_{SDW}, plotted against the incommensuration parameter $\delta = H - 0.5$. The solid line is a fit using a Gaussian with a linear background. (*B*) Integrated intensity of the SDW reflection vs. temperature. The dashed line shows the square-root fit used to determine T_{SDW} (main text). Error bars represent SEs. (*C*) Momentum scans in the *H* direction for all dopings at $T = 1.5$ K, except for $x = 0.11$, which was taken at 4 K. Solid lines are fits using a Gaussian with a linear background. The black tick above each curve indicates the peak position.

a peculiar dependence on doping and temperature: At $x = 0.10$, the CDW wavevector increases monotonically with temperature, while at $x = 0.20$ the wavevector monotonically decreases. At intermediate dopings, the peak shifts in a nonmonotonic manner, decreasing upon warming from the base temperature and then reversing and increasing at higher temperature. Note that our data agree well with the high-resolution resonant inelastic x-ray scattering (RIXS) study of LESCO $x = 0.125$ reported in ref. 19, in which the elastic scattering was measured directly (*SI Appendix*, section VI), validating that our observations are not influenced by the background subtraction method.

To quantify the CDW profiles, we fit the momentum scans at each temperature and doping with Lorentzian functions (*SI Appendix*, section V) to obtain the peak intensity, I_{peak}; correlation length, ξ; and x component of the wave vector, Q_{CDW}. ξ is defined as the inverse of the half width at half maximum of the CDW reflection peak. To be precise, $\xi = \left(\mathrm{HWHM} \cdot \frac{2\pi}{a}\right)^{-1}$, where a is the lattice parameter and HWHM is the half width at half maximum in reciprocal lattice units (r.l.u.). Figs. 2*B* and 3*A* show the temperature dependence of I_{peak} and ξ (black circles), illustrating a slow broadening of the CDW upon warming over a wide range of dopings. Wang et al. (19) observed the same behavior at $x = 0.125$ and concluded that the CDW persists far above the onset temperature reported by previous RSXS studies (18, 22, 23). Our result extends this conclusion to the entire doping range, where the CDW persists above the highest temperature measured at all compositions where it is observed.

The development of the CDW reflected in the temperature dependence of I_{peak} and ξ (Figs. 2*B* and 3*A*) does not adhere to expectations for a traditional mean-field phase transition. For all dopings, the evolution of the spectra is gradual and we do not find

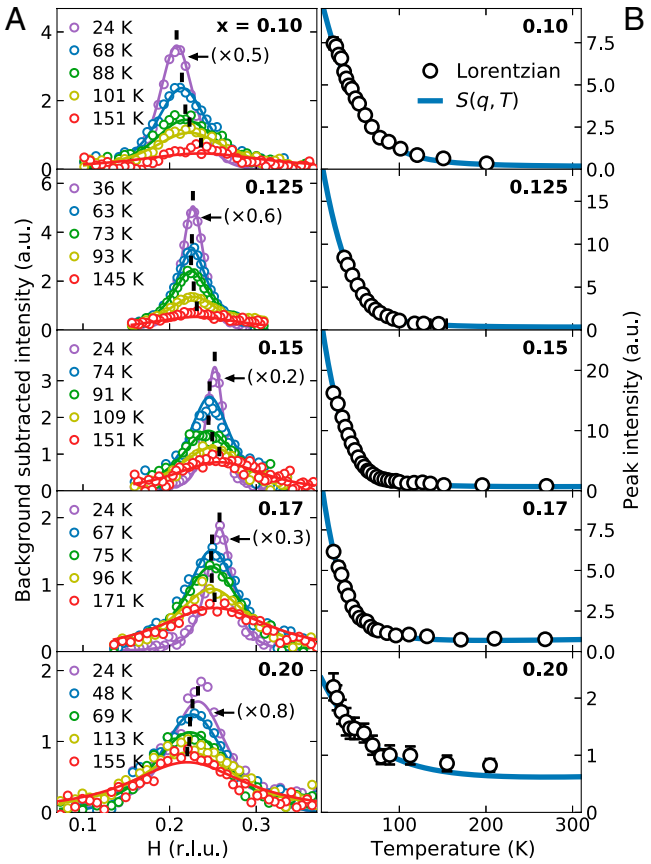

Fig. 2. RSXS measurements of the charge order in LESCO. (*A*) Momentum scans in the *H* direction at each doping where the CDW was observed for a selection of temperatures (fluorescence background has been subtracted). Solid lines are fits using $S(q, T)$ in Eq. **1**. The black tick above each curve indicates the fit peak position. (*B*) Temperature dependence of the CDW peak intensity obtained from fits using a Lorentzian function (open circles) and Eq. **1** (solid lines).

any indication of a sharp or even a rounded transition. This may suggest that the CDW is weak and that the spectra merely indicate incipient CDW fluctuations. Such an interpretation is, however, at odds with the significant correlation length, approaching ∼15 unit cells at low temperature (Fig. 3). A more plausible interpretation is that the nominal CDW transition temperature, in the absence of disorder, is higher than the highest temperatures measured. In this scenario, the amplitude of the CDW is already well formed at all temperatures measured, and the gradual evolution of the spectra reflects the coupling of disorder to the CDW and the suppression of phase fluctuations as temperature is reduced.

The latter perspective is supported by our finding that $I_{\text{peak}} \propto \xi^2$ over the range of measured temperatures (Fig. 3*B*). This behavior was first reported in ref. 19 for LESCO and several other La cuprates with $x = 0.125$ doping, and our results confirm this relationship over a wide range of doping from $x = 0.10$ to 0.20. The CDW in La cuprates is known to be essentially two-dimensional, with weak out-of-plane correlations (9, 24) and correlations in the (H, K) plane that are isotropic (9, 25). If a similar temperature dependence of the correlation length in the K direction is assumed, this suggests that the in-plane integrated intensity—a measure of the CDW amplitude—is essentially temperature independent.

For a quantitative test of whether phase fluctuations can account for the temperature dependence of the spectra, we consider a nonlinear sigma model as described in ref. 26 and *SI Appendix*, section VII. This model assumes that the amplitude of the CDW is formed at high temperatures. In the presence of a linear coupling between disorder (parameterized by σ) and the CDW order parameter, there is no true long-range order below four dimensions at any temperature (27). However, in the unbroken phase, the model predicts spectra with the lineshape

$$S(q, T) = TG(q, T) + \sigma^2 G^2(q, T), \quad [1]$$

where

$$G(q, T) = \frac{1}{\kappa q^2 + \mu(T)}. \quad [2]$$

Here, $q = Q - Q_{\text{CDW}}$ is momentum relative to Q_{CDW}, κ is the CDW stiffness, and $\mu(T) = \kappa\xi(T)^{-2}$, where $\xi(T)$ is the CDW correlation length. The temperature dependence of the lineshape is contained in $\mu(T)$, which is determined by

$$4\pi\kappa = T \ln\left[\frac{\Gamma}{\mu}\right] + \frac{\sigma^2}{\mu}, \quad [3]$$

which follows the self-consistency condition requiring the area under $S(q, T)$ be independent of T (*SI Appendix*, section VII). Note that this condition automatically accounts for the observed temperature-independent in-plane integrated intensity. Including an overall normalization factor, the model has only four free parameters. We find that for every doping, without introducing temperature dependence to the parameters, the model fits well to the entire two-dimensional set of data for $S(q, T)$ (*SI Appendix*, section V). Indeed, the solid lines in Figs. 2*B* and 3*A* compare remarkably well to the results of the Lorentzian fits (where parameters are temperature dependent), except for a few points at high temperature where the Lorentzian fits are not strongly constrained.

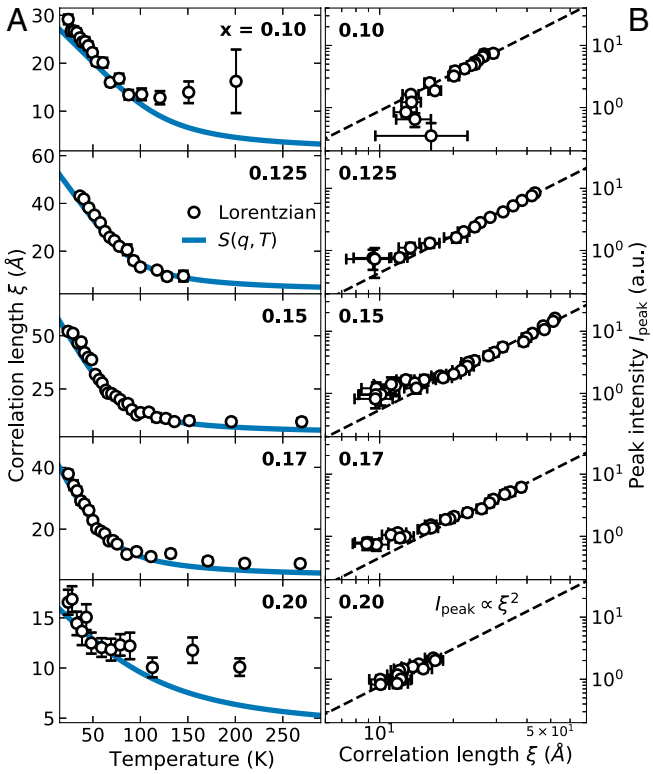

Fig. 3. Temperature dependence of the CDW linewidth at each doping. (*A*) Temperature dependence of the correlation length, ξ, obtained from a Lorentzian fit (open circles) compared to Eq. **1** (solid lines). (*B*) Peak intensity plotted against ξ on a log scale demonstrating that $I_{\text{peak}} \propto \xi^2$ (dashed lines represent a reference quadratic function).

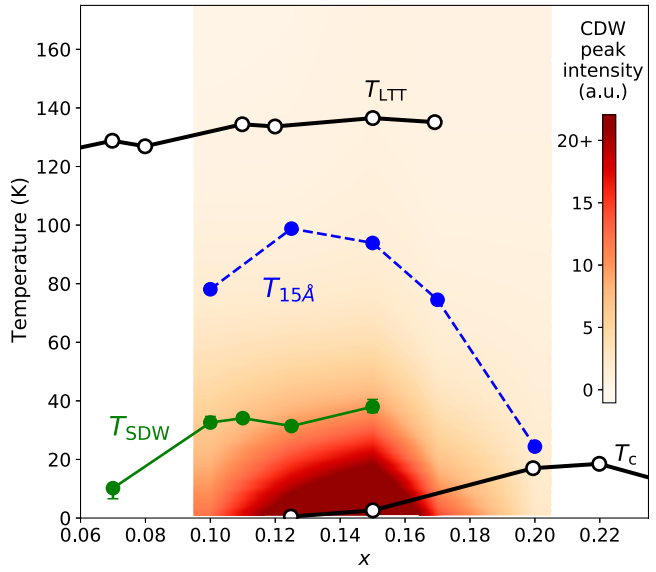

Fig. 4. Phase diagram of LESCO showing the SDW onset temperature T_{SDW} and the CDW cross-over temperature $T_{15Å}$ at which the correlation length takes the (arbitrary) value $\xi = 15$ Å. The overlaid color scale represents the CDW peak intensity. The LTT structural transition, T_{LTT}, and the superconducting transition, T_c, shown for reference, are taken from ref. 18.

This analysis strongly suggests that the temperature dependence of the lineshape is predominantly related to the effects of disorder on thermal phase fluctuations of the CDW, whose onset temperature is far above the highest temperature studied. While the CDW amplitude remains largely unchanged, at higher temperatures the correlations are short ranged due to strong phase fluctuations. At lower temperatures, disorder pins the fluctuations and the CDW correlation length grows.

We now consider the doping, x, at which the CDW is most stable. The transition temperature, T_{CDW}, is not a useful measure of stability because it is immeasurably high. The peak intensity (Fig. 4, color scale) is a better measure, but requires perfect calibration of the RSXS intensity between samples. For this reason, we found the best measure of the CDW stability to be a characteristic temperature, $T_{15Å}$, at which the correlation length takes the (arbitrary) value $\xi = 15$ Å (Fig. 4, blue points). This quantity can be compared directly between samples and exhibits a maximum at $x = 0.125$, similar to the previously reported CDW "phase boundary" in LESCO (18), as in other La cuprates (9, 10), for which the CDW onset temperatures were defined based on the peak intensity. We emphasize that $T_{15Å}$ is not a phase boundary but a cross-over scale and indicates that the CDW is optimized at $x \sim 1/8$ as in other La cuprates.

We now examine the nonmonotonic evolution of Q_{CDW}. Unlike I_{peak} and ξ, whose temperature dependences are similar at all dopings, Q_{CDW} exhibits a distinct behavior for different dopings. In Fig. 5, we display the evolution of Q_{CDW} as a function of x and T (black open circles). At the lowest doping $x = 0.10$, Q_{CDW} continuously increases upon warming from 0.208 r.l.u. at $T = 24$ K to 0.236 r.l.u. at $T = 200$ K. However, at higher dopings, a kink is present around $T \sim 75$ K where the trend of the temperature dependence changes: At $x = 0.15$, Q_{CDW} decreases from 0.251 r.l.u. at $T = 24$ K to 0.244 r.l.u. at $T = 78$ K and then increases to 0.261 r.l.u. at $T = 270$ K. The increasing trend above the kink becomes less pronounced at $x = 0.17$ and changes sign at $x = 0.20$, with Q_{CDW} decreasing over the entire temperature range from 0.233 r.l.u. at $T = 24$ K to 0.222 r.l.u. at $T = 207$ K, although a kink at $T \sim 60$ K is still present.

A monotonic shift of Q_{CDW} has been observed in several other stripe materials. In $La_{1.875}Ba_{0.125}CuO_4$, for example, Q_{CDW} moves away from its low-temperature value of 0.235 r.l.u. to a high temperature value of 0.272 r.l.u. at T = 90 K (12), while in $La_{2-x}Sr_xNiO_4$ Q_{CDW} shifts toward a commensurate value of 1/3 upon warming regardless of doping level (15). In both cases, it is believed that the coupling of the CDW to spin correlations causes Q_{CDW} to shift from an intrinsically favored high-temperature value as the temperature is reduced. However, the nonmonotonic evolution of Q_{CDW} found in our study is a different phenomenon, and it suggests that there are multiple competing effects at play.

Noting that the kink in the T dependence of Q_{CDW} occurs at temperatures comparable to the onset temperature of SDW order obtained from the neutron scattering results (Fig. 1) and that the mutual commensurability of CDW and SDW orders is known to be strong in La-based cuprates, we posit that the low-temperature behavior of Q_{CDW} is again related to the onset of SDW order. However, we attribute the behavior at intermediate T to other effects. While the microscopic mechanism of CDW order in cuprates is not fully understood, we can still describe the data by an effective theory. Because of the significant variation of Q_{CDW} with temperature and doping, even in the absence of SDW order, such a theory must account for the finite electronic compressibility of LESCO, i.e., that it has a finite conductivity in the temperature range of interest. Such a finite compressibility is known to influence the temperature dependence of a CDW ordering wavevector (20).

Thus, for a minimal theoretical description of the nonmonotonic behavior of Q_{CDW}, we start with the Landau–Ginzburg

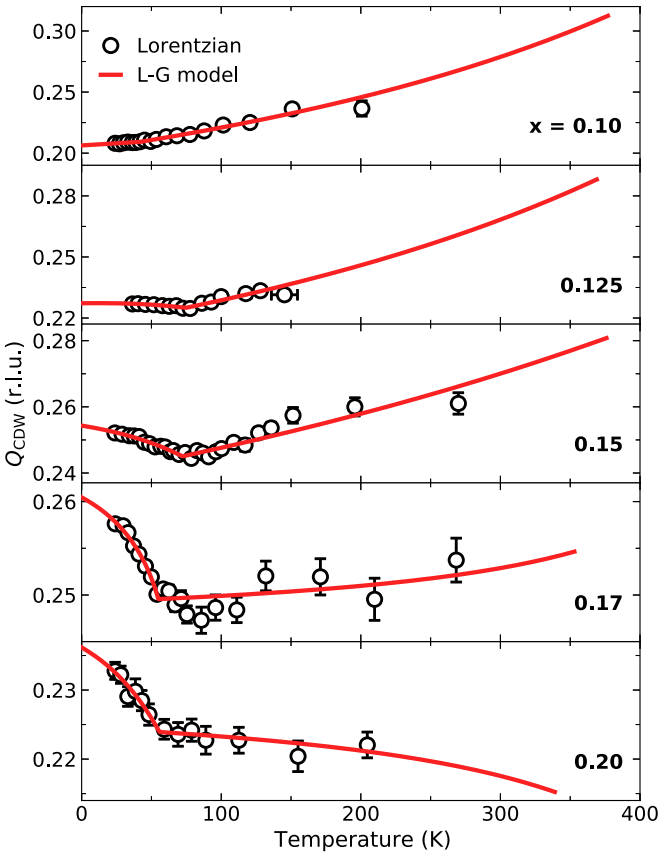

Fig. 5. Temperature dependence of Q_{CDW} obtained from Lorentzian fits (open circles) showing nonmonotonic behavior that reverses with doping. The solid lines are fits using the Landau–Ginzburg model described in the main text.

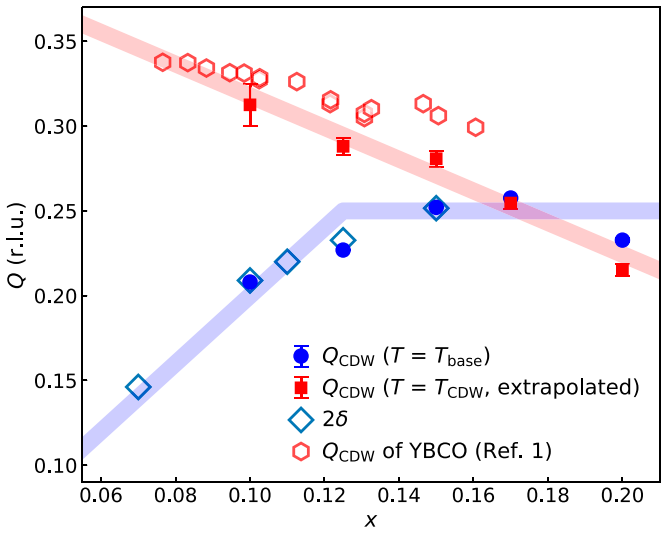

Fig. 6. Doping dependence of Q_{CDW} at our base temperature, T_{base} (solid blue circles), and extrapolated to $T = T_{CDW}$ (solid red squares) using the Landau–Ginzburg model described in the main text. The solid blue line represents the Yamada relation and the solid red line is a guide to the eye. Double the value of δ obtained from neutron scattering (Fig. 1*C*) (open blue diamonds) tracks Q_{CDW} at low temperature. The value of Q_{CDW} for YBCO from ref. 1 is shown for comparison (open red hexagons).

theory for an incommensurate CDW in a system with finite compressibility, following the approach of ref. 20. We include also the free energy of the SDW order and the CDW–SDW coupling. The latter produces a tendency to mutual commensurability of the CDW and SDW ordering wavevectors. The full expression for the free energy and its solution are given in *SI Appendix*, section VII.

We determine the CDW ordering wavevector by minimizing the free energy with respect to the CDW and SDW order parameters. For this purpose, we assume that the wavevector shift is uniform in space, i.e., does not occur through the formation of CDW discommensurations (28, 29). RSXS and neutron scattering are not sensitive to real space details of the order, and our Landau–Ginzburg theory gives similar predictions for both cases. The question of discommensurations therefore lies outside the scope of this study. The resulting temperature dependence of Q_{CDW}, generically, shows smooth behavior at high temperature and a kink near the SDW transition. It is reasonable to assume the parameters may depend on x although they should not change with T. A straightforward multiparameter optimization results in the fit curves in Fig. 5. These fits incorporated our knowledge from the earlier lineshape analysis (Fig. 2*A*), which showed that the integrated CDW intensity remains significant at the highest temperatures measured, by assuming a very high nominal CDW transition temperature $T_{CDW} = 400$ K. Note that the temperature of the kink, which in the theory occurs at the SDW transition, is slightly different from T_{SDW} determined from neutron scattering. This is because the spin transition is broadened so different measures of the transition yield different values.

Our model allows us to extrapolate the behavior of the CDW in LESCO to high temperature, near T_{CDW} (Fig. 6), where the spin order is absent and the amplitude of the CDW is small. These conditions allow a direct comparison to YBCO and Bi cuprates, in which the CDW amplitude is lower (30) and spin order is absent. Fig. 6 shows the value of Q_{CDW} at the base temperature, T_{base}, as well as at T_{CDW}, extrapolated using the Landau–Ginzburg model. At low temperature, Q_{CDW} follows the Yamada relationship (11), which can be understood as a result of the mutual commensurability between the CDW and the SDW.

The doping dependence at $T = T_{CDW}$ is, however, completely different: The extrapolated value of Q_{CDW} is close to 0.31 r.l.u. at $x = 0.10$ and continuously decreases with doping, reaching 0.22 r.l.u. at $x = 0.20$. Although the absolute values are slightly different, this trend mimics the behavior observed in YBCO and Bi-based compounds. This observation suggests that the behavior of Q_{CDW} in this La-based cuprate, if it could be measured at high temperature where its amplitude is small and the effect of the SDW is minimal, would follow the same phenomenology as YBCO and Bi-based cuprates.

Fig. 6 suggests that there is a universal CDW mechanism operating in all cuprates, which simply manifests differently in different materials because of extrinsic effects such as pinning on the SDW. The key ingredient included in our Landau–Ginzburg theory is the compressibility of the uncondensed electrons (20), which permits a proper determination of the effect of temperature on the CDW wavevector. We emphasize that we do not make any claim about the microscopic mechanism driving the CDW; our study shows only that the mechanism—whatever it is—is universal in all cuprates.

In summary, we carried out a comprehensive study of the CDW and SDW in isotopically enriched LESCO over a wide range of doping and temperature. The theoretical analysis of the RSXS data suggests that the CDW is formed at a much higher temperature than previously thought. The CDW is initially short ranged due to thermal phase fluctuations, and a cross-over takes place upon lowering temperature to a regime in which disorder pins the fluctuations and the CDW correlation length develops. We also identified the effect of charge compressibility that competes with the effect of CDW–SDW coupling, creating a nonmonotonic shift of Q_{CDW} with doping and temperature. The extrapolation of the Landau–Ginzburg model reveals that the doping dependence of Q_{CDW} at $T = T_{CDW}$ follows the same trend observed in YBCO and Bi-based cuprates. Our study suggests that the CDW is a generic phenomenon in hole-doped cuprates with a common formation mechanism that remains to be determined.

Materials and Methods

Sample Growth and Characterization. Single crystals of $La_{1.8-x}Eu_{0.2}Sr_xCuO_4$ with $x = 0.07$, 0.10, 0.11, 0.125, 0.15, 0.17, and 0.20 were grown by the traveling-solvent floating-zone technique. Naturally occurring europium has a large neutron absorption cross-section, which has impeded the study of spin order in LESCO using neutron scattering. To address this issue, we have grown isotopically enriched crystals using ^{153}Eu, which has a smaller neutron absorption cross-section than that of the natural abundance. This isotope did not have any noticeable effect on the electronic or magnetic properties of the crystals.

The hole-doping level of the crystals was controlled by the Sr concentration, and it was confirmed by comparing the measurements of the Sr and hole concentration. The Sr concentration was measured using energy-dispersive X-ray fluorescence (ED-XRF) measurements or inductively coupled plasma optical emission spectroscopy (ICP-OES); the two techniques gave identical Sr concentrations when measuring the same sample. To exclude other factors that may affect the hole doping, we also directly measured the hole concentration from the O K edge X-ray absorption spectra (XAS) (31). The XAS were measured in total fluorescence yield mode using a transition edge sensor (TES) array detector (32, 33), which provides an excellent detection efficiency, at beamline 13-3 of the Stanford Synchrotron Radiation Lightsource (SSRL). The measured hole doping p showed a good agreement with the Sr concentration x (*SI Appendix*, section II).

The Miller indexes (H, K, L) denote a momentum transfer wavevector $Q = (2\pi H/a, 2\pi K/b, 2\pi L/c)$ in a tetragonal unit cell, where the lattice parameters are $a = b = 3.79$ Å and $c = 13.14$ Å at $x = 0.125$. For the full doping dependence of the lattice parameters, see *SI Appendix*, section I.

RSXS Measurements. RSXS experiments at the Cu L_3 edge ($\sim$ 932 eV) were carried out at beamline 13-3 of the SSRL. The samples were cleaved in air to

expose the (0, 0, 1) surface before RSXS measurements, and the (H, 0, L) plane was aligned to the scattering plane inside the scattering chamber using a four-circle in-vacuum diffractometer. The CDW peak profiles along the in-plane momentum direction H were measured by performing scans of the sample angle θ with respect to the incident X-ray beam, while the detector was fixed at 120°. The samples were cooled using an open-cycle helium cryostat with a base temperature of T_{base} = 24 K, except for the x = 0.125 measurement, for which T_{base} = 36 K. To subtract fluorescence backgrounds accurately, and thereby to enhance sensitivity to scatterings from CDW, we employed a two-dimensional charge-coupled device (CCD) detector that measures CDW signals and backgrounds simultaneously. The background subtraction method is described in *SI Appendix*, section IV and also in ref. 34.

Neutron Scattering Measurements. Elastic neutron scattering measurements were performed using the HB-3 and HB-1A triple-axis spectrometers at the High Flux Isotope Reactor (HFIR) at Oak Ridge National Laboratory (ORNL). For HB-3, we used an incident energy of E = 14.7 meV and set collimators to 48′-60′-60′-120′; for HB-1A, we used an incident energy of E = 14.6 meV and set collimators to 40′-40′-40′-80′. We measured the samples with x = 0.07, 0.10, 0.11, 0.125, and 0.15 on HB-3, with additional data gathered on HB-1A only for samples x = 0.10, 0.125, and 0.15. These crystals were mounted in the (H, K, 0) scattering plane inside a helium cryostat with a base temperature of 1.5 K; we used a closed-cycle refrigerator with a base temperature of 4 K for the x = 0.11 sample. The data from HB-1A were scaled by an overall constant multiplication factor to match the data from HB3, and the two datasets agreed well with each other.

Data Availability. All data have been deposited in the Illinois Data Bank (https://doi.org/10.13012/B2IDB-1757317_V1).

ACKNOWLEDGMENTS. X-ray experiments were supported by the US Department of Energy, Office of Basic Energy Sciences (BES) Grant DE-FG02-06ER46285. Use of the SSRL was supported by Department of Energy (DOE) Contract DE-AC02-76SF00515. Neutron scattering experiments and growth of LESCO crystals were supported by DOE BES Grant DE-SC0012368. The neutron measurements used the High Flux Isotope Reactor, a DOE Office of Science User Facility operated by Oak Ridge National Laboratory. Theoretical work was supported by National Science Foundation Grant DMR-1725401 (to E.F.) and DOE BES Grant DEAC02-76SF00515 (to S.A.K.). We acknowledge support from the Gordon and Betty Moore Foundation's EPiQS Initiative through Grants GBMF9452 (to P.A.), GBMF4305 (to E.W.H.), and GMBF8691 (to E.W.H.).

Author affiliations: [a]Department of Physics, University of Illinois at Urbana–Champaign, Urbana, IL 61801; [b]Materials Research Laboratory, University of Illinois at Urbana–Champaign, Urbana, IL 61801; [c]Institute of Condensed Matter Theory, University of Illinois at Urbana–Champaign, Urbana, IL 61801; [d]Stanford Synchrotron Radiation Lightsource, SLAC National Accelerator Laboratory, Menlo Park, CA 94025; [e]National Institute of Standards and Technology, Boulder, CO 80305; [f]Neutron Scattering Division, Oak Ridge National Laboratory, Oak Ridge, TN 37831; and [g]Department of Physics, Stanford University, Stanford, CA 94305

Author contributions: G.J.M., E.F., and P.A. designed research; S.L., E.W.H., T.A.J., X.G., A.A.H., M.M., K.L., A.V.Z., G.A.d.l.P., Y.P., H.H., S.-J.L., H.J., J.-S.L., Y.I.J., W.B.D., P.S., D.S.S., S.C., A.A.A., G.J.M., S.A.K., E.F., and P.A. performed research; S.L., E.W.H., T.A.J., G.J.M., S.A.K., E.F., and P.A. analyzed data; and S.L., E.W.H., T.A.J., S.A.K., E.F., and P.A. wrote the paper.

1. R. Comin, A. Damascelli, Resonant x-ray scattering studies of charge order in cuprates. *Annu. Rev. Condens. Matter Phys.* **7**, 369–405 (2016).
2. G. Ghiringhelli *et al.*, Long-range incommensurate charge fluctuations in (Y,Nd)$Ba_2Cu_3O_{6+x}$. *Science* **337**, 821–825 (2012).
3. E. Blackburn *et al.*, X-ray diffraction observations of a charge-density-wave order in superconducting Ortho-II $YBa_2Cu_3O_{6.54}$ single crystals in zero magnetic field. *Phys. Rev. Lett.* **110**, 137004 (2013).
4. M. Hücker *et al.*, Competing charge, spin, and superconducting orders in underdoped $YBa_2Cu_3O_y$. *Phys. Rev. B Condens. Matter Mater. Phys.* **90**, 054514 (2014).
5. R. Comin *et al.*, Charge order driven by Fermi-arc instability in $Bi_2Sr_{2-x}La_xCuO_{6+\delta}$. *Science* **343**, 390–392 (2014).
6. K. Fujita *et al.*, Spectroscopic imaging scanning tunneling microscopy studies of electronic structure in the superconducting and pseudogap phases of cuprate high-T_c superconductors. *J. Phys. Soc. Jpn.* **81**, 011005 (2012).
7. E. H. da Silva Neto *et al.*, Ubiquitous interplay between charge ordering and high-temperature superconductivity in cuprates. *Science* **343**, 393–396 (2014).
8. P. Abbamonte *et al.*, Spatially modulated 'Mottness' in $La_{2-x}Ba_xCuO_4$. *Nat. Phys.* **1**, 155–158 (2005).
9. M. Hücker *et al.*, Stripe order in superconducting $La_{2-x}Ba_xCuO_4$ ($0.095 \leqslant x \leqslant 0.155$). *Phys. Rev. B Condens. Matter Mater. Phys.* **83**, 104506 (2011).
10. T. P. Croft, C. Lester, M. S. Senn, A. Bombardi, S. M. Hayden, Charge density wave fluctuations in $La_{2-x}Sr_xCuO_4$ and their competition with superconductivity. *Phys. Rev. B Condens. Matter Mater. Phys.* **89**, 224513 (2014).
11. K. Yamada *et al.*, Doping dependence of the spatially modulated dynamical spin correlations and the superconducting-transition temperature in $La_{2-x}Sr_xCuO_4$. *Phys. Rev. B Condens. Matter Mater. Phys.* **57**, 6165–6172 (1998).
12. H. Miao *et al.*, High-temperature charge density wave correlations in $La_{1.875}Ba_{0.125}CuO_4$ without spin–charge locking. *Proc. Natl. Acad. Sci. U.S.A.* **114**, 12430–12435 (2017).
13. L. Nie, A. V. Maharaj, E. Fradkin, S. A. Kivelson, Vestigial nematicity from spin and/or charge order in the cuprates. *Phys. Rev. B* **96**, 085142 (2017).
14. H. Miao *et al.*, Formation of incommensurate charge density waves in cuprates. *Phys. Rev. X* **9**, 031042 (2019).
15. R. Kajimoto *et al.*, Hole concentration dependence of the ordering process of the stripe order in $La_{2-x}Sr_xNiO_4$. *Phys. Rev. B Condens. Matter Mater. Phys.* **64**, 144432 (2001).
16. H. H. Klauss *et al.*, From antiferromagnetic order to static magnetic stripes: The phase diagram of $(La, Eu)_{2-x}Sr_xCuO_4$. *Phys. Rev. Lett.* **85**, 4590–4593 (2000).
17. M. Fujita, H. Goka, K. Yamada, M. Matsuda, Competition between charge- and spin-density-wave order and superconductivity in $La_{1.875}Ba_{0.125-x}Sr_xCuO_4$. *Phys. Rev. Lett.* **88**, 167008 (2002).
18. J. Fink *et al.*, Phase diagram of charge order in $La_{1.8-x}Eu_{0.2}Sr_xCuO_4$ from resonant soft x-ray diffraction. *Phys. Rev. B Condens. Matter Mater. Phys.* **83**, 092503 (2011).
19. Q. Wang *et al.*, High-temperature charge-stripe correlations in $La_{1.675}Eu_{0.2}Sr_{0.125}CuO_4$. *Phys. Rev. Lett.* **124**, 187002 (2020).
20. S. E. Brown, E. Fradkin, S. A. Kivelson, Surface pinning of fluctuating charge order: An extraordinary surface phase transition. *Phys. Rev. B Condens. Matter Mater. Phys.* **71**, 224512 (2005).
21. M. Hücker *et al.*, Coupling of stripes to lattice distortions in cuprates and nickelates. *Physica C: Superconductivity and Its Applications* **460–462**, 170–173 (2007).
22. J. Fink *et al.*, Charge ordering in $La_{1.8-x}Eu_{0.2}Sr_xCuO_4$ studied by resonant soft x-ray diffraction. *Phys. Rev. B Condens. Matter Mater. Phys.* **79**, 100502 (2009).
23. A. J. Achkar *et al.*, Nematicity in stripe-ordered cuprates probed via resonant x-ray scattering. *Science* **351**, 576–578 (2016).
24. N. B. Christensen *et al.*, Bulk charge stripe order competing with superconductivity in La2–xSrxCuO4 (x = 0.12). arXiv:1404.3192 (11 April 2014).
25. S. B. Wilkins *et al.*, Comparison of stripe modulations in $La_{1.875}Ba_{0.125}CuO_4$ and $La_{1.48}Nd_{0.4}Sr_{0.12}CuO_4$. *Phys. Rev. B Condens. Matter Mater. Phys.* **84**, 195101 (2011).
26. L. Nie, G. Tarjus, S. A. Kivelson, Quenched disorder and vestigial nematicity in the pseudogap regime of the cuprates. *Proc. Natl. Acad. Sci. U.S.A.* **111**, 7980–7985 (2014).
27. Y. Imry, S.-k. Ma, Random-field instability of the ordered state of continuous symmetry. *Phys. Rev. Lett.* **35**, 1399–1401 (1975).
28. W. L. McMillan, Theory of discommensurations and the commensurate-incommensurate charge-density-wave phase transition. *Phys. Rev. B* **14**, 1496 (1976).
29. G. Grüner, *Density Waves in Solids* (Perseus, Cambridge, MA, 1994).
30. E. Fradkin, S. A. Kivelson, J. M. Tranquada, Colloquium: Theory of intertwined orders in high temperature superconductors. *Rev. Mod. Phys.* **87**, 457–482 (2015).
31. C. T. Chen *et al.*, Electronic states in $La_{2-x}Sr_xCuO_{4+\delta}$ probed by soft-x-ray absorption. *Phys. Rev. Lett.* **66**, 104–107 (1991).
32. W. B. Doriese *et al.*, A practical superconducting-microcalorimeter X-ray spectrometer for beamline and laboratory science. *Rev. Sci. Instrum.* **88**, 053108 (2017).
33. Y. I. Joe *et al.*, Resonant soft x-ray scattering from stripe-ordered $La_{2-x}Ba_xCuO_4$ detected by a transition-edge sensor array detector. *Phys. Rev. Appl.* **13**, 034026 (2020).
34. J. J. Wen *et al.*, Observation of two types of charge-density-wave orders in superconducting $La_{2-x}Sr_xCuO_4$. *Nat. Commun.* **10**, 3269 (2019).